Environmental Science Processes & Impacts

Mandelic Acid and Phenyllactic Acid "Reaction Sets" for Exploring the Kinetics and Mechanism of Oxidations by Hydrous Manganese Oxide (HMO)

Journal:	*Environmental Science: Processes & Impacts*
Manuscript ID	EM-ART-03-2019-000128.R1
Article Type:	Paper
Date Submitted by the Author:	30-Apr-2019
Complete List of Authors:	Xia, Xiaomeng; Johns Hopkins University - Homewood Campus, Environmental Health and Engineering Stone, Alan; Johns Hopkins University - Homewood Campus, Environmental Health and Engineering

Mandelic Acid and Phenyllactic Acid "Reaction Sets" for Exploring the Kinetics and Mechanism of Oxidations by Hydrous Manganese Oxide (HMO)

Xiaomeng Xia, Alan T. Stone

Department of Environmental Health and Engineering

Whiting School of Engineering

Johns Hopkins University

Baltimore, MD 21218

Submitted to: *Environmental Science: Processes & Impacts*, February 11, 2019

Graphical Abstract

Two hydroxy acids reaction sets are used to explore the kinetics, the role of physicochemical properties, and medium effects of the heterogenerious reactions on hydrous manganese oxide (HMO) surface.

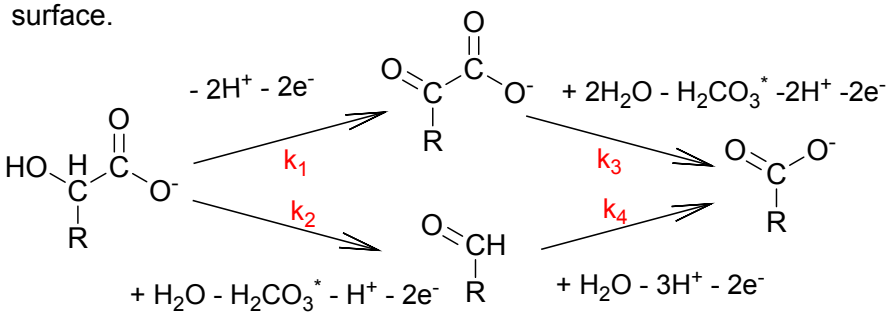

Abstract

At pH 4.0, hydrous manganese oxide (HMO) oxidizes mandelic acid by two mole-equivalents of electrons, yielding phenylglyoxylic acid and benzaldehyde. These intermediates, in turn, are oxidized by two mole-equivalents of electrons to the same ultimate oxidation product, benzoic acid. The four compounds of the "reaction set" just described are conveniently monitored using capillary electrophoresis (CE) and HPLC. Extents of adsorption are negligible and their sum exhibits mass balance. Concentrations of phenylglyoxylic acid, benzaldehyde, and benzoic acid can therefore be used to calculate mole-equivalents delivered to HMO for comparison with experimentally-determined dissolved Mn^{II} concentrations. Semi-log plots (ln[substrate] versus time) and numerical analysis can also be used to explore rates of oxidation of the functional groups represented, i.e. an α-hydroxycarboxylic acid, an α-ketocarboxylic acid, and an aldehyde. Inserting a $-CH_2-$ group between the benzene ring and the functional groups just described yields a new reaction set comprised of phenyllactic acid, phenylpyruvic acid, and phenylacetaldehyde, plus the C-1 ultimate oxidation product, phenylacetic acid. At pH 4, mass balance for phenyllactic acid oxidation fell short by ~ 9 %. Phenyllactic acid was oxidized 2.7-times more slowly than mandelic acid, while phenylpyruvic acid was oxidized 12.7-times faster than phenylglyoxylic acid. Unlike benzaldehyde, oxidation rates for phenylacetaldehyde were too fast to measure. Under pH 4.0 conditions, this reaction set approach was used to explore the acceleratory effects of increases in HMO loading and inhibitory effects of 500 μM phosphate and pyrophosphate additions. Mandelic acid and phenyllactic acid were oxidized by HMO far more slowly at pH 7.0 than at pH 4.0. At pH 7.0, 2 mM MOPS and phosphate buffers did not yield appreciable dissolved Mn^{II}, despite oxidation of organic substrate. 2 mM Pyrophosphate, in contrast, solubilized HMO-bound Mn^{II} and Mn^{III}.

Environmental significance

Within surface waters, soils, and sediments, manganese oxyhydroxides likely serve as reactive sinks for siderophores and other natural products that contain α-hydroxycarboxylic acid, α-ketocarboxylic acid, and aldehyde functional groups. These aliphatic functional groups also likely contribute to the reductant capacity and reactivity of natural organic matter (NOM). Within water supply plants, HMO generated through permanganate reduction or through Mn^{II} oxidation by chlorine, chloramines, ozone, and other disinfectants may convert α-hydroxycarboxylic acids into α-ketocarboxylic acids and aldehydes, and α-ketocarboxylic acids and aldehydes into carboxylic acids. By altering the suite of organic compounds present, identities and amounts of disinfection byproducts generated by downstream processes may be altered.

1. Introduction

Manganese oxyhydroxides are important transitional redox zone oxidants, found within the water column of stratified lakes, inlets, and seas, as nodules, dendrites, and crusts within soils, and as nodules and crusts at sediment-water interfaces.[1-3] In water supply plants, manganese oxyhydroxides are formed when O_2, permanganate, and commonly-employed disinfectants (e.g., chlorine, chloramines, ozone) oxidize Mn^{2+}.[4-6] Many organic compounds are oxidized rapidly by manganese oxyhydroxides. Although a great deal is known about oxidations of phenol- and aniline-bearing contaminants, relatively little is known about oxidations of compounds bearing aliphatic reductant groups.[7]

To learn more about the reactivities of important aliphatic reductant groups with manganese oxyhydroxides, we have selected two "reaction sets" depicted in Figure 1. Each contributing compound possesses a benzene ring that facilitates UV detection, but is not itself oxidized or reduced by manganese oxyhydroxides. Compounds in the phenyllactic acid reaction set possess a -CH_2- group located between the benzene ring and the oxidizable moieties, while those in the mandelic acid reaction set do not. With each set we will quantify hydroxy acid, keto acid, and C-1 acid by capillary electrophoresis, and aldehyde by HPLC.

The eight organic compounds comprising the two reaction sets are representative of a great many other organic compounds with widespread occurrence and considerable environmental significance, briefly outlined in Electronic Supplementary Information (S1). The electrophilicity of keto acids and aldehydes is particularly noteworthy. It has been established that pyruvic acid, oxaloacetic acid, and α-ketoglutaric acid protect cell cultures from *in situ* generated hydrogen peroxide by forming adducts that irreversibly break down into the corresponding C-1 acid and bicarbonate ion.[8-13] Comparable reactions have been confirmed for phenylglyoxylic acid[14] and phenylpyruvic acid.[15] Keto acid groups generated through oxidation of hydroxy acids within natural organic matter (NOM) may similarly serve as sinks for hydrogen peroxide. Aldehydes like benzaldehyde and phenylacetaldehyde, do not serve in a protective role, but instead may be toxic.[16]

Electronic effects arising from the phenyl or benzyl groups of the compounds shown in Figure 1 will be addressed in this work. Many cured-in-place pipe (CIPP) formulations are styrene-based. The two styrene oxidation products included in our study, benzaldehyde and benzoic acid, have been associated with CIPP installation.[17, 18] 4-Hydroxy-3-methoxymandelic acid has been detected during lignin degradation by white rot fungus.[19, 20] (4-Hydroxy-3-

methoxyphenyl)-glyoxylic acid is generated during the polysulfide treatment of lignin.[21] These two examples from the wood, pulp, and paper literature should not come as a surprise, given that lignin is the product of biologically controlled radical coupling of the hydroxy-/methoxy-substituted styrenes coniferyl alcohol, sinapyl alcohol, and coumaryl alcohol.[22, 23]

Our objective is to show how reaction set organic substrates can be used to explore the kinetics of heterogeneous redox reactions. The hydrous manganese oxide (HMO) that we use as oxidant, formed from the oxidation of Mn^{2+} by MnO_4^-, is typical of the low crystallinity δ-MnO_2 found in soils, sediments, and water supply plants. Simultaneous monitoring of hydroxy acid, keto acid, aldehyde, and C-1 acid concentrations as a function of time is a central feature of this work. As noted in Figure 1, electron mole-equivalents transferred in each of the four reaction steps are known. If we can demonstrate that these compounds do not adsorb significantly to manganese oxyhydroxides and that mass balance involving the four compounds in each set is achieved, then we have the means of determining electron mole-equivalents delivered to manganese oxyhydroxides. We will also employ semi-log plots (ln[substrate] versus time) and numerical analysis to obtain rates and rate constants for the four reaction steps. This provides a basis for exploring medium effects, e.g. effects of added phosphate and pyrophosphate and changes to suspension pH. Comparing results of the mandelic acid reaction set with those of the phenyllactic acid reaction set will shed light on electronic effects arising from the aromatic ring.

2. Materials and Methods

All solutions and suspensions were prepared using 18 MΩ•cm resistivity distilled, deionized water (DDW, Millipore Corp., Milford, MA). All bottles and glassware were rinsed

with distilled water, soaked in 5 M HNO_3 (J. T. Baker, Phillipsburg, NJ) overnight, rinsed with distilled water, and then rinsed with DDW and air dried prior to use. Glassware, bottles, and filter holders having prior contact with HMO solutions were first soaked in 1 M ascorbic acid (Aldrich, Milwaukee, WI) and were rinsed several times with DDW prior to soaking in 5 M HNO_3.

2.1. Chemicals

All chemical reagents were of the highest purity available. Mandelic acid was obtained from Acros Organics (NJ) with the purity of 99%. Phenylglyoxylic acid with the purity of 95%, benzoic acid with the purity of 99.5%, benzaldehyde with the purity of 99+%, phenyllactic acid with the purity of 98+%, phenylpyruvic acid with the purity of 98%, and phenylacetic acid with the purity of 99% were purchased from Sigma-Aldrich (St. Louis, MO). Phenylacetaldehyde was purchased from Alfa Aesar with the putiry of 95%. Ionic strength was adjusted using NaCl (Acros Organics). Sodium hydroxide, acetic acid, hydrochloric acid, and sodium acetate were purchased from J. T. Baker and used to buffer pH. These buffers were selected because they are poorly oxidized by HMO and complex metals weakly, and therefore do not consume HMO or influence Mn speciation during the reactions. 3-[N-morpholino] propanesulfonic acid (MOPS, Sigma-Aldrich), Na_2HPO_4 (J. T. Baker), and $Na_2H_2P_2O_7$ (Sigma-Aldrich) were used as buffers at pH 7.0.

2.2. HMO Synthesis and Characterization

HMO (hydrous manganese oxide) synthesis began by heating a 4.0×10^{-3} M $NaMnO_4$ (Sigma-Aldrich) and 1.0×10^{-2} M NaOH (J. T. Baker) solution (0.5 L) to 90 ^{o}C in a 1 L glass Erlenmeyer flask. A 6.5×10^{-3} M $MnCl_2.4H_2O$ (Sigma-Aldrich) solution (0.5 L) was then added

dropwise by manually adjusting the stopcock of a separatory funnel. After addition was complete, the suspension was maintained at 90 °C for an additional two hours, and then allowed to cool to room temperature. Eight different preparations supplied the HMO for our experiments (Table S1). To minimize the effect of particle aging, each preparation was used within two weeks of synthesis. We used the same reagents as Murray[24], and similar concentrations. We elected, however, to add a slight stoichiometric excess of Mn^{II}, and did not use dilution/resuspension to lower the ionic strength of the suspensions produced. Most importantly, synthesis and early aging were performed at 90 °C, while Murray employed room temperature.

To determine the total concentration of HMO in the suspension, 100 mL of HMO suspension was transferred to a polypropylene bottle and reduced by an excess amount of ascorbic acid, then the total dissolved Mn was measured using flame atomic absorption spectrophotometry (AAS, AAnalyst 100, Perkin-Elmer, Norwalk, CT). Since dissolved Mn of filtered HMO suspension was consistently below the detection limit of 1 μM, the total dissolved Mn concentration measured after ascorbic acid reduction is equal to the concentration of HMO. The average oxidation state of manganese was determined by iodometric titration for two of the HMO preparations.[25] 10 mL of HMO suspension was transferred to a 50 mL Erlenmeyer flask, and reduced by an excess amount of KI (Fisher Chemical, Pittsburgh, PA) in 0.01 M HCl solution. When the solution became a brown I_3^- solution, the flask was wrapped with aluminum foil and incubated in the dark for 2 minutes. The brown I_3^- solution was back-titrated using 0.01 M $Na_2S_2O_3$ solution (Fisher Chemical). Right before the end point was reached, several drops of soluble starch indicator (Fisher Chemical) was added, yielding a blue color. The titration was continued, with the endpoint corresponding to the point where the suspension became colorless. The titration was repeated twice for each HMO suspension. For both HMO suspensions tested,

the average oxidation state was found to be +3.82. If we assume that Mn^{II} is not present, then this average oxidation state corresponds to 18 % Mn^{III} and 82 % Mn^{IV}.

2.3. Experimental Design

All experiments were conducted in 100 mL polypropylene bottles to prevent adsorption of metal ions to reactor surfaces. All reactions were conducted in a constant temperature water bath at 25 ºC ± 0.1 ºC and stirred with Teflon-coated stir bars. Constant pH was maintained using 5 mM acetate (pH 4.0), MOPS (pH 7.0), phosphate (pH 7.0), or pyrophosphate (pH 7.0) buffer, and constant ionic strength was maintained using 10 mM NaCl. Stability of solution pH was verified by periodic measurement (Fisher Accumet 825MP meter with Orion Combination semi-micro probe; NIST-traceable standards).

The reaction solutions were prepared by first mixing together pH buffer, electrolyte, and organic substrate from aqueous stock solutions. No efforts were taken to exclude molecular oxygen from the reaction suspension. The reactions were initiated by adding HMO. The initial concentration of organic substrate in most kinetic experiments was 50 μM, and HMO was present in considerable excess (0.5 mM). 4mL reaction suspension aliquots were collected at periodic intervals as the reactions proceeded. Filtration using 0.05 μm pore diameter track-etched polycarbonate membranes (Whatman) was used to quantitatively remove HMO particles, quenching the reaction. Filtered solutions were analyzed by AAS for total Mn and by capillary electrophoresis (CE) for organic species (see later section). As noted before, when filtered, dissolved Mn in HMO suspensions lacking organic substrates was consistently below this detection limit. Organic substrates and intermediates reduce HMO to Mn^{II}, but are not strong enough chelating agents to solubilize Mn^{III} or Mn^{IV}. We can therefore assume that dissolved

manganese consists entirely of Mn^{II}. Medium containing pyrophosphate is an important exception, owing to the ability of pyrophosphate to chelate and solubilize Mn^{III}.[26-29]

2.4. Organic Analysis

A CE system (Sciex, P/ACE MDQ) with diode-array UV-visible detector was used for analyzing ionized organic compounds. Bare fused silica capillaries (Polymicro Technologies, Phoenix, AZ) with 75 μm ID and 60 cm total length were used for all separations. The effective length defined as the length from the inlet to the detector was 52 cm. $NaH_2PO_4.H_2O$ (J. T. Baker), Na_2HPO_4 (J. T. Baker), and "electroosmotic flow modifier" tetradecyltrimethylammonium chloride (TTAC) (Sigma-Aldrich) were used in the back ground electrolyte (BGE) buffer. BGE buffer contained 25 mM phosphate (pH 7.0), and 0.5 mM TTAC. Between separations, the capillary was sequentially rinsed by pressure flushing DDW for 1 minute, 0.1 M NaOH for 1 minute, DDW for 1 minute, and BGE buffer for 2 minutes. Anion mode with constant applied voltage (-25 kV) was employed for all separations. Sample injection employed 0.5 psi of positive pressure for 15 seconds. All analyses were conducted at 25 ºC in the constant temperature chamber within the instrument. Data were collected at a detection wavelength of 194 nm. Since peak area can be affected by the velocity of the sample, peak areas were calibrated by dividing them by the migration time.[30] Typical detection limits for the organic anions reported here was approximate 1 μM. Representative electropherograms are shown in Figure S8 and S9. Based on the comparison of electropherograms between filtered reaction solution and authentic standards, the three peaks are assigned to carboxylic acid, keto acid and hydroxy acid in each reaction set, respectively.

Concentrations of the neutral organic species benzaldehyde and phenylacetaldehyde were determined using reverse-phase HPLC with UV detection at 238 nm. An HPLC system (Waters

Corp., Milford, MA) was used with a μ-Bondapac column (3.9 × 300 mm column containing 5 μm C_{18} packing material). The flow rate was set at 1 mL/min and an isocratic eluent (5 mM acetic acid (J. T. Baker) in 15% acetonitrile (J. T. Baker) /85% H_2O v/v) was used. The injection volume was 200 μL. A representative chromatogram is shown in Figure S10.

2.5. Data Analysis

We applied the following kinetic model to our time course results:

$$\frac{dA_T}{dt} = -k_1 A_T - k_2 A_T \quad (1)$$

$$\frac{dW_T}{dt} = k_1 A_T - k_3 W_T \quad (2)$$

$$\frac{dY_T}{dt} = k_2 A_T - k_4 Y_T \quad (3)$$

$$\frac{dB_T}{dt} = k_3 W_T + k_4 Y_T \quad (4)$$

A_T, W_T, Y_T, and B_T refer to total dissolved concentrations of hydroxy acid, keto acid, aldehyde, and final carboxylic acid product, respectively. Consequently, under each set of reaction conditions, it will be necessary to evaluate whether the reactions shown in Figure 1 actually follow pseudo-first-order behavior. When the hydroxy acid serves as substrate, the sum ($k_1 + k_2$) can be obtained as the slope of log(A_T) versus time plots. When the keto acid serves as substrate, k_3 can be obtained from plots of log(W_T) versus time. When the aldehyde serves as substrate, k_4 can be obtained from plots of log(Y_T) versus time.

Distinguishing k_1 from k_2 is desirable, but in order to do this, we need information about keto acid and aldehyde time course behavior. Concentrations of keto acid and aldehyde as a function of time aren't determined by source reactions alone; sink reactions, i.e. oxidation of keto

acid and aldehyde to C-1 acid, must also be accounted for. Fortunately, the software package SCIENTIST for Windows (v. 3.0, Micromath, Salt Lake City, UT) is available for numerically fitting entire A_T, W_T, Y_T, and B_T versus time data sets. The apportionment and optimization approach implemented by SCIENTIST yields ($k_1 + k_2$), k_3 and k_4 values that can then be compared with values obtained from plots of $\log(A_T)$, $\log(W_T)$, and $\log(Y_T)$ versus time.

3. Results and Discussion

3.1. Mandelic Acid Reaction Set: Time Course and Stoichiometries

The mandelic acid reaction set corresponds to -R in Figure 1 being a phenyl group (-C_6H_5). Reactions at mineral/water interfaces evolve differently from reactions in homogeneous solution owing to possible site-site reactivity variability and chemical changes to the surface that accompany reaction. Effects of these phenomena should become more acute as the HMO loading is decreased.

As shown in Figure 2, hydroxy acid loss rates decreased substantially as the HMO loading was decreased from 500 to 200, and finally to 100 μM. Keto acid concentrations reached a maximum (20 μM) at 7.5 hours when the loading was 500 μM. Lowering the HMO loading to 200 μM did not appreciably affect the concentration achieved at the maximum, but the maximum occurred later, at 15 hours. Lowering the HMO loading still further to 100 μM yielded a plateau, also at 20 μM, during late stages of the experiment. Presumably the keto acid concentration would have reached a maximum and then declined if the duration of the experiment had been longer. The aldehyde concentrations reached a plateau at all three HMO loadings. There was a modest decrease in this plateau as the HMO loading was decreased, and the plateau was reached

later in the time course when lower HMO loadings were used. C-1 acid concentrations followed S-shaped curves. Inflection points in these curves occurred at later times as the HMO loading was decreased, and the C-1 concentration achieved by the end of each experiment decreased as well. This S-shaped profile confirmed that C-1 acid is derived from oxidation of keto acid and aldehyde intermediates and not from direct oxidation of hydroxy acid parent; keto acid and aldehyde concentrations must build up before appreciable rates of C-1 acid production can occur. As shown in the figure, summing the concentrations of the four reaction set compounds yielded good mass balance at all three HMO loadings, indicating that adsorption of hydroxy acid, keto acid, aldehyde, and C-1 acid was negligible.

Reaction stoichiometry is important for understanding HMO loading effects. Based upon the experimentally measured average Mn oxidation state of +3.82, we can represent the manganese half-reaction as:

$$MnO_{1.91}(s) + 3.82H^+ + 1.82e^- = Mn^{II} + 1.91H_2O \quad (5)$$

Turning our attention to the mandelic acid reaction set, each oxidation step depicted in Figure 1 corresponds to an organic half reaction: one mole of hydroxy acid oxidized to either keto acid or aldehyde yields two moles of electrons; one mole hydroxy acid oxidized to C-1 acid yields four moles of electrons. Adding organic half-reactions to the manganese half reaction yields three full reactions:

$$RCH(OH)COO^- + 1.10MnO_{1.91} + 2.20H^+ = RC(O)COO^- + 1.10Mn^{2+} + 2.10H_2O \quad (6)$$

$$RCH(OH)COO^- + 1.10MnO_{1.91} + 3.20H^+ = RC(O)H + 1.10Mn^{2+} + H_2CO_3^* + 1.10H_2O \quad (7)$$

$$RCH(OH)COO^- + 2.20MnO_{1.91} + 4.40H^+ = RCOO^- + 2.20Mn^{2+} + H_2CO_3^* + 2.20H_2O \quad (8)$$

(Derivations are shown in Supporting Information S2.) The fact that mandelic acid reaction set compounds do not adsorb to any appreciable extent means that experimentally-determined keto

acid, aldehyde, and C-1 acid concentrations provide a means of predicting the amount of Mn^{II} generated, denoted using RS for "reaction set":

$$[Mn]_{RS} = 1.10\times[\text{keto acid}] + 1.10\times[\text{aldehyde}] + 2.20\times[\text{C-1 acid}] \quad (9)$$

$[Mn]_{RS}$ can then be compared with $[Mn]_{diss}$, the quantity obtained by filtering reaction aliquots followed by AAS analysis. Strong chelating agents were not employed in the experiments presented in this section. Hence, dissolved Mn^{III} and Mn^{IV} are negligible, and $[Mn]_{diss}$ should consist entirely of Mn^{II}.[29]

As shown in Figure 3, $[Mn]_{diss}/[Mn]_{RS}$ was low at the onset of the reaction employing 500 μM HMO, but gradually approached 1.0 during 35 hours of reaction. When 200 μM HMO was employed, the early discrepancy between $[Mn]_{diss}$ and $[Mn]_{RS}$ was lower, and the ratio approached 1.0 sooner, within 20 hours of reaction. When 100 μM HMO was employed, only the first reaction aliquot showed significant discrepancy between $[Mn]_{diss}$ and $[Mn]_{RS}$.

Descrepancies between $[Mn]_{diss}$ and $[Mn]_{RS}$ seen in Figure 3 indicate that particle-bound Mn^{III} or Mn^{II} is present. Mn^{II} adsorption largely explains the discrepancies seen in Figure 3 between $[Mn]_{diss}$ and $[Mn]_{RS}$. Mn^{II} adsorption onto HMO can be significant even at pH values as low as 4.0 and at HMO loadings comparable to those employed here.[31] Under neutral and alkaline conditions and at strongly acidic pH, adsorbed Mn^{II} is known to engage in conproportionation reactions with oxyhydroxide-bound Mn^{IV}, generating oxyhydroxide-bound Mn^{III} [32-34] and thereby trapping reducing equivalents within HMO particles. Conproportionation reactions are not, however, believed to be important near pH 4.[33, 35]

At the end of the reaction employing 500 μM HMO, $[Mn]_{RS}$ was found equal to 80 μM, i.e. 16 % of total added manganese. The corresponding value for our 200 μM HMO experiments

was 60 μM, 30 % of total added manganese. For the 100 μM HMO experiments, the value was 34 μM, 34 % of total added manganese. Comparable decreases in the net volume of HMO particles in suspension likely took place. We can conclude that alteration of the remaining HMO surface was least important when the HMO loading was 500 μM, and more important in experiments employing lower HMO loadings.

We can also initiate reactions mid-way in the mandelic acid reaction set by using phenylglyoxylic acid (Figure 4A) or benzaldehyde (Figure 4B) as substrate. Good mass balance ([substrate] + [C-1 acid]) was obtained in both cases. During each time course, dissolved Mn concentrations matched or slightly exceeded concentrations of C-1 acid product. Carefully taking into account the average oxidation state of HMO and calculating $[Mn]_{diss}/[Mn]_{RS}$ (Figures S12 D and E) reveals that the ratio is again low at the onset of reaction, but gradually approaches 1.0 as each reaction progresses.

3.2. Mandelic Acid Reaction Set: Rates and Rate Constants

As noted in Materials and Methods, $(k_1 + k_2)$ can be obtained from slopes of ln[hydroxy acid] versus time plots, k_3 from slopes of ln[keto acid] versus time plots, and k_4 from slopes of ln[aldehyde] versus time plots (employing hydroxy acid, keto acid, and aldehyde, respectively, as added substrate). When 500 μM HMO loadings were employed, semi-log plots were linear throughout each time course (Figures 2D, 4D, 4E, and S11), and hence under these conditions it is reasonable to assume that hydroxy acid, keto acid, and aldehyde consumption were pseudo-first-order.

Lowering HMO loadings to 200 and 100 μM resulted in semi-log plots that, while initially linear, exhibited increasing curvature (more pronounced decreases in rates) during later

stages of reaction. As noted in the preceding section, percentages of HMO consumed between 30 and 34 % were observed during 35 hours of reaction when these HMO loadings were employed. Significant loss of HMO surface sites or diminishment of the reactivity of remaining sites are entirely reasonable explanations. Although strictly not obeying pseudo-first-order behavior, we elected to apply this assumption in a limited number of cases for the sake of comparison. Assuming that the four contributing reactions are pseudo-first-order simplifies numerical modeling employing SCIENTIST 3.0.

Recall that concentrations of all four reaction set organic compounds as a function of time were included in the SCIENTIST fitting exercise. In Figure 2C, k_1, k_2, k_3, and k_4 values obtained from 500 μM HMO data were used to generate time course simulations. The simulated concentrations and the experimental data agree quite nicely. Simulations can be used to show how rates of the four contributing reactions changed as reaction progressed. As shown in Figure 2F, the time when r_1 and r_3 crossed corresponded to the maximum in keto acid concentration. r_4 was so low that it never crossed r_2. For this reason, a plateau in aldehyde concentration was observed, not a maximum.

Fitting parameters obtained from the 500 μM HMO experiment yielded excellent fits for the first 10 hours of the 100 μM HMO and 200 μM HMO time course data (Figure 2A-B). At later portions of these two runs, however, fitting parameters from the 500 μM HMO experiment yielded hydroxy acid loss rates that were too high, keto acid maxima that were too high, and aldehyde plateau values that were too high. We can conclude that at these two lower HMO loadings significant consumption of surface sites took place, or that the reactivity of remaining sites diminished as reaction progressed.

Quite interestingly, using SCIENTIST to extract fitting parameters from 100 μM HMO experiments and applying fits to 100 μM HMO data yielded initial rates of hydroxy acid consumption (and production of keto acid and aldehyde) during the first ten hours that were too low (Figure S13A). Fitting parameters obtained from 200 μM HMO experiments applied to 200 μM HMO data similarly yielded initial rates that were too low (Figure S13B). Explaining these results is straightforward. Fitting parameters from the 500 μM HMO experiment nicely capture the reactivity of pristine surface sites. SCIENTIST fitting to 100 and 200 μM HMO experimental data includes data points collected late in the experiments where the surface sites are no longer pristine and surface site loadings have diminished. These late data points spoil the fit to early portions of data.

When 500 μM HMO was employed, ($k_1 + k_2$) values obtained by semi-log lot (0.256 (±0.007) hr^{-1}) and by SCIENTIST fitting (0.269 (±0.023) hr^{-1}) are in reasonable agreement. SCIENTIST additionally indicates that hydroxy acid oxidation to keto acid (with k_1 = 0.19 (±0.01) hr^{-1}) was 2.4-times faster than hydroxy acid oxidation to aldehyde (k_2 = 7.91 (±0.95) $\times 10^{-2}$ hr^{-1}). The two intermediates were ultimately oxidized to C-1 acid. The keto acid (k_3 = 7.03 (±0.40) $\times 10^{-2}$ hr^{-1}) was 34-times more reactive than the aldehyde (k_4 = 2.06 (±0.22) $\times 10^{-3}$ hr^{-1}). When keto acid and aldehyde were used as substrates, values obtained from semi-log plots (7.35 (±0.70) $\times 10^{-2}$ hr^{-1} for k_3 and 2.22 (±0.21) $\times 10^{-3}$ hr^{-1} for k_4) and values obtained from SCIENTIST fitting are in good agreement.

Dividing rate constants by HMO loading (in $mole \cdot L^{-1}$) yields normalized rate constants (k_1', k_2', k_3', k_4') compiled in Table 1 that facilitate comparisons of results obtained using different HMO loadings. Despite normalization, values of all four normalized rate constants

consistently increased as the HMO loading was increased. Again, significant loss of HMO surface sites or diminishment of the reactivity of remaining sites at the lower loadings are likely explanations.

The balance between two competitive reactions in parallel can be evaluated using normalized rate constants. As shown below, the ratio of hydroxy acid oxidation to keto acid versus hydroxy acid oxidation to aldehyde increases as the HMO loading is decreased:

HMO Loading	k_1'/k_2'
100 μM	2.9
200 μM	2.6
500 μM	2.2

Keto acid oxidation to C-1 acid versus aldehyde oxidation to C-1 acid also makes for interesting comparison:

HMO Loading	k_3'/k_4'
100 μM	-
200 μM	40
500 μM	34

(Aldehyde oxidation in the 50 μM mandelic acid plus 100 μM HMO experiment was too slow for SCIENTIST to obtain a value for k_4'.) By altering rates of reactions that both produce intermediates (keto acid and aldehyde) and consume them (yielding C-1 acid), changes in HMO loadings bring about significant changes to organic species time course behavior, as shown in Figure 2.

3.3. Phenyllactic Acid Reaction Set

The phenyllactic acid reaction set corresponds to -R in Figure 1 being a benzyl group (-$CH_2C_6H_5$), i.e. with an added methylene group between the aromatic ring and the reactive portion of each molecule. As shown in Figure 5A, hydroxy acid loss rates were lower than observed in the mandelic acid experiment performed under comparable conditions (Figure 2C). Experimental keto acid concentrations were barely above the detection limit. The maximum keto acid concentration was 13-times lower than observed in the corresponding mandelic acid experiment, and occurred at 2.5 hours, not at 8 hours. Aldehyde concentrations were below the detection limit throughout the experiment. Although concentrations of phenylacetic acid, the C-1 acid product, increased as concentrations of phenyllactic acid decreased, mass balance fell short, by approximately 9 %. As far as reaction stoichiometry is concerned, relationships analogous to Equations 6-9 apply. Early in the reaction, discrepancies between $[Mn]_{diss}$ and $[Mn]_{RS}$ (Figure 5B) are slightly smaller than those observed in the mandelic acid experiment under comparable conditions (Figure 3C). The ratio $[Mn]_{diss}/[Mn]_{RS}$ (Figure 5D) nears unity a little sooner than observed in the mandelic acid experiment (Figure 3F).

The value of $(k_1 + k_2)$ obtained using semi-log plots was 7-times lower when phenyllactic acid served as substrate than when mandelic acid served as substrate. Phenylpyruvic acid is the keto acid for this reaction set. When used as substrate (Figure 4C), phenylpyruvic acid was 12.7-times more reactive towards HMO than phenylglyoxylic acid, the keto acid of the mandelic acid reaction set. During the 2.5 hour duration of our experiments employing phenylpyruvic acid as a substrate, the sum of [keto acid] and [C-1 acid] decreased 10 %. This missing mass balance is of the same magnitude as the missing mass balance seen when phenyllactic acid was used as substrate. $[Mn]_{RS}$, calculated from measurements of phenylpyruvic acid and C-1 acid

concentrations, fell considerably short of $[Mn]_{diss}$ (Figure S12F). We hypothesize that the portion missing from mass balance arises from oxidation of phenylpyruvic acid to a product that is not detected by CE, and that generation of this product yields more than two electron-equivalents.

Phenylacetaldehyde, the aldehyde for the phenyllactic acid reaction set, is at least five orders-of-magnitude more reactive towards HMO than benzaldehyde, the aldehyde for the mandelic acid reaction set. Oxidation of phenylacetaldehyde by HMO was so fast that phenylacetaldehyde could not be detected in an aliquot collected at 1 minute, immediately filtered and injected into HPLC. The C-1 acid concentration in this sample, measured by CE, equaled the concentration of phenylacetaldehyde reactant used. $[Mn]_{diss}$ of this sample was 53.2 μM measured by AAS, which is agreement with $[Mn]_{RS}$ (55 μM), calculated using the measured C-1 acid concentration and Reaction S10 of Supporting Information.

3.4. Organic Reactivity Comparisons

The two mechanisms for mandelic acid oxidation by transition metal-containing species that have been presented in the literature are shown in Figure S14. In Scheme I, mandelic acid oxidation begins with hydrogen atom abstraction, which generates a free radical intermediate.[36, 37] In Scheme II, mandelic acid oxidation begins with hydride ion transfer, which generates a carbocation intermediate.[36, 38] Electronic interactions with the benzene ring would be expected to stabilize free radical or carbocation intermediates generated from mandelic acid oxidation relative to those generated from phenyllactic acid oxidation. Although we cannot establish which oxidation mechanism is operative, the higher reactivity of mandelic acid in comparison with phenyllactic acid is reasonable.

The keto acid phenylpyruvic acid can form gem-diols via hydration and can form enols (Figure S15). Although thermodynamic information isn't available for phenylpyruvic acid, it is available for pyruvic acid, and their speciation should be similar. As discussed in Supporting Information S3, the two gem-diols (HX^o and X^-) represent 7.7 % of the total pyruvic acid concentration at pH 4.0; only one molecule in 73,000 is found in one of the enol forms. The keto acid phenylglyoxylic acid, in contrast, can form gem-diols via hydration but cannot form enols. Gem-diols only comprise 0.1 % of total phenylglyoxylic acid at pH 4.0. Gem-diols have been reported to be much more readily oxidized than corresponding keto forms. Hence, the 13-fold higher reactivity of phenylpyruvic acid in comparison to phenylglyoxylic acid is quite reasonable.

Phenylacetaldehyde can form a gem-diol via hydration and can also form *cis*- and *trans*-enols. According to Chiang et al.,[39] the gem-diol represents 75 % of total phenylacetaldehyde in solution, whereas only one molecule in 2850 exists in one of the enol forms. Only about 0.8 % of total benzaldehyde is found in the gem-diol form, and formation of an enol is not possible.[40, 41] The preponderance of the more oxidizable gem-diol of phenylacetaldehyde, and its high reactivity towards oxidants, quite readily explains why it doesn't appear when phenyllactic acid serves as substrate, and why it is entirely consumed by the time the first aliquot is collected when added as substrate.

3.5. pH 4.0 Experiments with Added Phosphate and Pyrophosphate

In our next set of experiments (Figure 6), we continued to maintain pH 4.0 using 5.0 mM acetate, but augmented the reaction medium with ten-fold lower concentrations (500 μM) of phosphate or pyrophosphate. Linear regression of the logarithm of the mandelic acid concentration as a function of time indicated that phosphate lowered the rate of mandelic acid

oxidation by 49 %, and pyrophosphate lowered the rate by 80 %. Rate constants for each step in the reaction set were derived from experimentally measured concentrations and included in Table 1. As shown in Figure S17, numerical simulations based on these rate constants fit time course data reasonably well. k_1 (conversion of hydroxy acid to keto acid) and k_2 (conversion of hydroxy acid to aldehyde) are lowered by phosphate and pyrophosphate additions to similar extents. k_3, the rate constant for conversion of keto acid into C-1 acid, decreased 56 % when phosphate was added, and 83 % when pyrophosphate was added. k_4, the rate constant for conversion of aldehyde into C-1 acid, was already low in the absence of additive. Phosphate and pyrophosphate diminished k_4 to negligible levels.

In control experiments free of organic substrate, neither 500 μM phosphate nor 500 μM pyrophosphate yielded any appreciable dissolved Mn after 30 hours of reaction. In mandelic acid-containing suspensions, Equation 9 can be used to convert measured concentrations of keto acid, aldehyde, and C-1 acid into $[Mn]_{RS}$, the expected amount of Mn^{II} generated by redox reaction, which can be compared with direct $[Mn]_{diss}$ measurements. As noted earlier, $[Mn]_{diss}$ falls significantly short of $[Mn^{II}]_{RS}$ throughout the entire time course when a 500 μM HMO loading is used and mandelic acid is added in the absence of phosphate or pyrophosphate. $[Mn]_{diss}/[Mn]_{RS}$ plotted as a function of time makes this discrepancy easier to discern (Figure 6G). In the presence of 500 μM pyrophosphate, a slight discrepancy is observed, but only in the earliest four data points. In the presence of 500 μM phosphate, a slightly larger discrepancy is seen, but it is again restricted to the earliest data points.

Phosphate and pyrophosphate effects on reaction pathways and rates likely arise from their coordination properties: (i) adsorption onto HMO surface sites, which lowers site accessibility to reductants, (ii) ligand-assisted dissolution of surface-bound Mn^{II} and Mn^{III}, and

(iii) formation of dissolved Mn^{II} and Mn^{III} complexes. Adsorption of phosphate and other oxyanions onto HMO at acid, neutral, and slightly alkaline pH is surprisingly robust, given that pH_{zpc} values for these materials are less than 4.[42] Villalobos[43] attributed this adsorption to oxyanion-reactive sites at sheet edges, and stated that they are relatively few in number in comparison to cation-reactive vacancy sites within basal planes. Being relatively few in number would be relevant to ligand-assisted dissolution, since Mn^{III}-oxyanion complexes are also attracted to these sites. Wang and Stone[29] concluded that pyrophosphate concentrations in excess of 1 mM must be added before all oxyanion-reactive sites are occupied, forcing Mn^{III}-oxyanion complexes into solution. Apparently phosphate and pyrophosphate concentrations in the experiments described in this section were too low for this to occur.

The tendency for Mn^{II} to adsorb or precipitate is less than that for Mn^{III}. Both phosphate and pyrophosphate are viable ligands for Mn^{II}, and can bring about release of surface-bound Mn^{II}, as reflected in nearly equal values of $[Mn]_{RS}$ and $[Mn]_{diss}$ observed when 500 μM phosphate and pyrophosphate are present.

3.6. pH 7 Experiments: MOPS, Phosphate, and Pyrophosphate Buffers

Mandelic acid and phenyllactic acid oxidation by HMO was also investigated at pH 7.0 in suspensions buffered using 2.0 mM MOPS, phosphate, or pyrophosphate**.** In MOPS and phosphate buffer, concentrations of dissolved Mn obtained by filtering reaction solutions and measured by AAS stayed below the detection limit throughout the duration of each experiment. As shown in Figure 7, the time courses for mandelic acid oxidation in MOPS and phosphate buffer look very similar, with keto acid as the only organic product detected, with good mass balance. Slopes of ln[mandelic acid] versus time yielded rate constants of 4.89 (±0.11) $\times 10^{-3}$ $hour^{-1}$ in MOPS buffer and 5.40 (±0.15) $\times 10^{-3}$ $hour^{-1}$ in phosphate buffer (Figure S18). This

amounts to a 50-fold decrease in the rate of mandelic acid loss in comparison to the pH 4.0 experiments presented earlier.

At pH 7.0, 2.0 mM phosphate yielded a rate of phenyllactic loss that was 1.43-times higher and produced twice as much keto acid than was observed in 2.0 mM MOPS (Figures 7 and S18). Concentrations of phenylacetic acid produced in the two reaction suspensions were approximately the same, and no aldehyde production was observed. Good mass balanced was obtained. On average, phenyllactic acid was oxidized 30-fold more slowly at pH 7.0 than at pH 4.0.

Unlike results obtained using MOPS and phosphate buffers, pH 7.0 pyrophosphate experiments produced substantial concentrations of dissolved manganese (Figure 8). In an organic substrate-free control experiment, ~ 5 % of total added HMO became dissolved during the first 6 hours. Between 6 and 150 hours, further dissolved manganese was released, but only added an additional 1.5 %. The total amount of manganese released in the control experiment, 33 μM, was a little more than one-third of the HMO Mn^{III} content at the loading employed (500 μM). UV/visible spectra of filtered solutions exhibited a peak at 260 nm (Figure S19A), matching a peak reported by other investigators in the $6.5 \leq pH \leq 8$ range,[26, 28, 29, 44] attributed to dissolved Mn^{III}-pyrophosphate complexes. Linear regression of absorbance versus dissolved manganese yielded a molar absorptivity of 6.17×10^3 $M^{-1}cm^{-1}$ (Figure S19D), which matches the pH 6.7 value reported by Cabelli and Bielski[44] (6.2×10^3 $M^{-1}cm^{-1}$).

In the presence of 50 μM mandelic acid or phenyllactic acid (Figure 8A,B) time courses for dissolved manganese during the first six hours of reaction were nearly the same as observed in the organic substrate-free control experiment. From six hours to the end of each experiment,

however, substantially greater increases in dissolved manganese were observed. The peak at 260 nm attributable to Mn^{III}-pyrophosphate complexes was observed and increased substantially during both experiments. Absorbance versus $[Mn]_{diss}$ was linear within early portions of each time course, but at later times exhibited downward curvature (Figure S19E,F). We elected to use the calibration curve obtained from the organic substrate-free experiment (Figure S19D) to calculate $[Mn^{III}]_{diss}$ organic substrate-containing experiments (Figure 8D,E). Substracting $[Mn^{III}]_{diss}$ from $[Mn]_{diss}$ yielded $[Mn^{II}]_{diss}$. At the end of the mandelic acid experiment, 17 % of dissolved manganese was Mn^{II} and 83 % was Mn^{III}. At the end of the phenyllactic acid experiment, 12 % was Mn^{II} and 88 % was Mn^{III}.

Mandelic acid and phenyllactic acid loss were slightly faster when pyrophosphate replaced MOPS or phosphate as buffer (Figure 8). Mandelic acid oxidation again yielded only keto acid. Phenyllactic acid oxidation yielded both keto acid and C-1 acid. Pyrophosphate was similar to phosphate in that keto acid production was twice that obtained when MOPS served as buffer. In all experiments employing 2 mM pyrophosphate buffer, good mass balanced was obtained.

Pyrophosphate exhibited the ability to "mine" a portion of the Mn^{III} content of the HMO suspensions employed, and yielded quite substantial dissolved Mn^{II} and Mn^{III} concentrations as reactions with mandelic acid and phenyllactic acid progressed. The fact that rates of organic substrate loss and identities/yields of oxidized products changed so little is rather surprising. We can speculate that hydroxy acid, keto acid, and aldehyde oxidations by HMO-bound Mn^{IV} are far more rapid than oxidations by HMO-bound Mn^{III} or by the dissolved Mn^{III}-pyrophosphate complexes that predominate at the pH and pyrophosphate concentration employed here. Removing HMO-bound Mn^{III} apparently had little effect on the reactivity of the remaining Mn^{IV}.

4. Conclusions

At pH 4.0, the reaction set comprised of mandelic acid, phenylglyoxylic acid, benzaldehyde, and benzoic acid exhibited mass balance during oxidations by HMO, and extents of adsorption were negligible. We were therefore able to calculate mole-equivalents delivered to HMO for comparison with experimentally-determined dissolved Mn^{II} concentrations. Because concentrations of phenylglyoxylic acid and benzaldehyde were appreciable and exhibited distinctive time course behavior, it was possible using numerical approaches to distinguish and quantify rates of contributing reactions occurring in series and in parallel. With phenyllactic acid, concentrations of phenylpyruvic acid were near the detection limit and concentrations of phenylacetaldehyde were not discernible. There was more and more deviation from mass balance as reactions progressed. Nevertheless, the phenyllactic acid reaction set revealed important aspects of α-hydroxycarboxylic acid, α-ketocarboxylic acid, and aldehyde reactivity. The inserted $-CH_2-$ group either raised the extent of hydration, yielding gem-diols, or raised the extent of tautomerization, yielding enols. Gem-diols and enols are far more reactive towards oxidants like HMO than corresponding keto forms.

Environmentally-relevant redox reactions are often far from simple. The reaction set approach entails finding the means of distinguishing and quantifying all reaction intermediates and products, so that contributing reaction steps can be fully and clearly discerned. We have demonstrated the utility of this approach for documenting HMO loading effects and effects of 500 μM phosphate and pyrophosphate on reactions at pH 4.0, and the effects of 2 mM phosphate and pyrophosphate on reactions at pH 7.0. In our subsequent publications, we will use the

reaction set approach to explore HMO-driven autocatalysis during permanganate oxidations, and other catalytic effects on permanganate oxidations.

References

1. J. E. Post, Manganese oxide minerals: crystal structures and economic and environmental significance, *Proc. Natl. Acad. Sci. U. S. A.*, 1999, **96**, 3447-3454.
2. B. M. Tebo, J. R. Bargar, B. G. Clement, G. J. Dick, K. J. Murray, D. Parker, R. Verity and S. M. Webb, Biogenic manganese oxides: properties and mechanisms of formation, *Annu. Rev. Earth Planet. Sci.*, 2004, **32**, 287-328.
3. P. A. J. Lusty, J. R. Hein and P. Josso, Formation and occurrence of ferromanganese crusts: earth's storehouse for critical metals, *Elements*, 2018, **14**, 313-318.
4. W. R. Knocke, R. C. Hoehn and R. L. Sinsabaugh, Using alternative oxidants to remove dissolved manganese from waters laden with organics, *J. - Am. Water Works Assoc.*, 1987, **79**, 75-79.
5. D. A. Reckhow, W. R. Knocke, M. J. Kearney and C. A. Parks, Oxidation of iron and manganese by ozone, *Ozone: Sci. Eng.*, 1991, **13**, 675-695.
6. J. E. Tobiason, A. Bazilio, J. Goodwill, X. Y. Mai and C. Nguyen, Manganese removal from drinking water sources, *Curr. Pollut. Rep.*, 2016, **2**, 168-177.
7. C. K. Remucal and M. Ginder-Vogel, A critical review of the reactivity of manganese oxides with organic contaminants, *Environ. Sci.: Processes Impacts*, 2014, **16**, 1247-1266.
8. E. Melzer and H. L. Schmidt, Carbon isotope effects on the decarboxylation of carboxylic acids. Comparison of the lactate oxidase reaction and the degradation of pyruvate by H_2O_2, *Biochem. J.*, 1988, **252**, 913-915.
9. L. H. Long and B. Halliwell, Artefacts in cell culture: α-ketoglutarate can scavenge hydrogen peroxide generated by ascorbate and epigallocatechin gallate in cell culture media, *Biochem. Biophys. Res. Commun.*, 2011, **406**, 20-24.
10. L. H. Long and B. Halliwell, The effects of oxaloacetate on hydrogen peroxide generation from ascorbate and epigallocatechin gallate in cell culture media: potential for altering cell metabolism, *Biochem. Biophys. Res. Commun.*, 2012, **417**, 446-450.
11. C. Asmus, O. Mozziconacci and C. Schoneich, Low-temperature NMR characterization of reaction of sodium pyruvate with hydrogen peroxide, *J. Phys. Chem. A*, 2015, **119**, 966-977.
12. A. Lopalco, G. Dalwadi, S. Niu, R. L. Schowen, J. Douglas and V. J. Stella, Mechanism of decarboxylation of pyruvic acid in the presence of hydrogen peroxide, *J. Pharm. Sci.*, 2016, **105**, 705-713.
13. A. Lopalco and V. J. Stella, Effect of molecular structure on the relative hydrogen peroxide scavenging ability of some α-keto carboxylic acids, *J. Pharm. Sci.*, 2016, **105**, 2879-2885.
14. B. Siegel and J. Lanphear, Kinetics and mechanisms for the acid-catalyzed oxidative decarboxylation of benzoylformic acid, *J. Org. Chem.*, 1979, **44**, 942-946.
15. A. Perera, H. G. Parkes, H. Herz, P. Haycock, D. R. Blake and M. C. Grootveld, High resolution ^{1}H NMR investigations of the reactivities of α-keto acid anions with hydrogen peroxide, *Free Radical Res.*, 1997, **26**, 145-157.
16. R. M. LoPachin and T. Gavin, Molecular mechanisms of aldehyde toxicity: a chemical perspective, *Chem. Res. Toxicol.*, 2014, **27**, 1081-1091.
17. S. M. T. Sendesi, K. Ra, E. N. Conkling, B. E. Boor, M. Nuruddin, J. A. Howarter, J. P. Youngblood, L. M. Kobos, J. H. Shannahan, C. T. Jafvert and A. J. Whelton, Worksite

chemical air emissions and worker exposure during sanitary sewer and stormwater pipe rehabilitation using cured-in-place-pipe (CIPP), *Environ. Sci. Technol. Lett.*, 2017, **4**, 325-333.

18. K. Ra, S. M. T. Sendesi, J. A. Howarter, C. T. Jafvert, B. M. Donaldson and A. J. Whelton, Critical review: surface water and stormwater quality impacts of cured-in-place pipe repairs, *J. - Am. Water Works Assoc.*, 2018, **110**, 15-32.
19. C. Chen, H. Chang and T. K. Kirk, Aromatic-acids produced during degradation of lignin in spruce wood by phanerochaete-chrysosporium, *Holzforschung*, 1982, **36**, 3-9.
20. R. F. P. Nogueira, R. A. Pilli and N. Duran, Degradation of *β*-O-4 lignin model and related-compounds by the ascomycete *chrysonilia-sitophila* (TFB-27441 strain), *Appl. Biochem. Biotechnol.*, 1992, **33**, 169-176.
21. F. Berthold, C. T. Lindgren and M. E. Lindstrom, Formation of (4-hydroxy-3-methoxyphenyl)-glyoxylic acid and (4-hydroxy-3,5-dimethoxyphenyl)-glyoxylic acid during polysulfide treatment of softwood and hardwood, *Holzforschung*, 1998, **52**, 197-199.
22. M. Ragnar, C. T. Lindgren and N. O. Nilvebrant, pK_a-values of guaiacyl and syringyl phenols related to lignin, *J. Wood Chem. Technol.*, 2000, **20**, 277-305.
23. L. Pollegioni, F. Tonin and E. Rosini, Lignin-degrading enzymes, *FEBS J.*, 2015, **282**, 1190-1213.
24. J. W. Murray, Surface chemistry of hydrous manganese-dioxide, *J. Colloid Interface Sci.*, 1974, **46**, 357-371.
25. E. W. Rice, Baird, R.B., Eaton, A. D., Clesceri, L. S., editors, *Standard Methods for the Examination of Water and Wastewater.*, American Public Health Association, American Water Works Association, Water Environment Federation, 22nd ed., 2012.
26. J. E. Kostka, G. W. Luther and K. H. Nealson, Chemical and biological reduction of Mn(III)-pyrophosphate complexes - potential importance of dissolved Mn(III) as an environmental oxidant, *Geochim. Cosmochim. Acta*, 1995, **59**, 885-894.
27. J. K. Klewicki and J. J. Morgan, Kinetic behavior of Mn(III) complexes of pyrophosphate, EDTA, and citrate, *Environ. Sci. Technol.*, 1998, **32**, 2916-2922.
28. J. K. Klewicki and J. J. Morgan, Dissolution of β-MnOOH particles by ligands: Pyrophosphate, ethylenediaminetetraacetate, and citrate, *Geochim. Cosmochim. Acta*, 1999, **63**, 3017-3024.
29. Y. Wang and A. T. Stone, Phosphonate- and carhoxylate-based chelating agents that solubilize (hydr)oxide-bound Mn(III), *Environ. Sci. Technol.*, 2008, **42**, 4397-4403.
30. D. R. Baker, *Capillary Electrophoresis*, John Wiley & Sons, Inc., New York, US, 1995.
31. J. W. Murray, Interaction of metal-ions at manganese dioxide solution interface, *Geochim. Cosmochim. Acta*, 1975, **39**, 505-519.
32. E. J. Elzinga, Reductive transformation of birnessite by aqueous Mn(II), *Environ. Sci. Technol.*, 2011, **45**, 6366-6372.
33. E. J. Elzinga, ^{54}Mn radiotracers demonstrate continuous dissolution and reprecipitation of vernadite (δ-MnO_2) during interaction with aqueous Mn(II), *Environ. Sci. Technol.*, 2016, **50**, 8670-8677.
34. H. Y. Zhao, M. Q. Zhu, W. Li, E. J. Elzinga, M. Villalobos, F. Liu, J. Zhang, X. H. Feng and D. L. Sparks, Redox reactions between Mn(II) and hexagonal birnessite change its layer symmetry, *Environ. Sci. Technol.*, 2016, **50**, 1750-1758.

35. J. P. Lefkowitz, A. A. Rouff and E. J. Elzinga, Influence of pH on the reductive transformation of birnessite by aqueous Mn(II), *Environ. Sci. Technol.*, 2013, **47**, 10364-10371.
36. F. Freeman and M. A. H. Scott, Permanganate oxidations. 5. Kinetics and mechanisms of oxidation of mandelate anions, *J. Org. Chem.*, 1970, **35**, 2989-2994.
37. D. G. Lee and T. Chen, The oxidation of alcohols by permanganate - a comparison with other high-valent transition-metal oxidants, *J. Org. Chem.*, 1991, **56**, 5341-5345.
38. R. S. Shukla, R. J. Verma and D. N. Mehta, Kinetic and mechanistic investigations on reduictions of aflatoxins by lactic acid, *Bioorg. Med. Chem. Lett.*, 2002, **12**, 2737-2741.
39. Y. Chiang, A. J. Kresge, P. A. Walsh and Y. Yin, Phenylacetaldehyde and its *cis*- and *trans*-enols and enolate ions. Determination of the *cis:trans* ratio under equilibrium and kinetic control, *J. Chem. Soc., Chem. Commun.*, 1989, **13**, 869-871.
40. W. J. Bover and P. Zuman, Lewis acid properties of benzaldehydes and substituent effects, *J. Chem. Soc., Perkin Trans. 2*, 1973, **6**, 786-790.
41. R. A. McClelland and M. Coe, Structure reactivity effects in the hydration of benzaldehydes, *J. Am. Chem. Soc.*, 1983, **105**, 2718-2725.
42. W. S. Yao and F. J. Millero, Adsorption of phosphate on manganese dioxide in seawater, *Environ. Sci. Technol.*, 1996, **30**, 536-541.
43. M. Villalobos, in *Advances in the Environmental Biogeochemistry of Manganese Oxides*, American Chemical Society, 2015, **1197**, 65-87.
44. D. E. Cabelli and B. H. J. Bielski, Pulse-radiolysis study of the kinetics and mechanisms of the reactions between manganese(II) complexes and HO_2/O_2^- radicals. 1. Sulfate, formate, and pyrophosphate complexes, *J. Phys. Chem.*, 1984, **88**, 3111-3115.

Figures and Tables

Table 1. Medium conditions and rate constants for the oxidation of the four organic substrates comprising the mandelic acid and phenyllactic acid reaction sets. Rate constants have been normalized with respect to HMO loading ($k_i' = k_i \div [HMO]$). Values in brackets were obtained from slopes of ln[substrate] as a function of time. The remaining values were obtained using SCIENTIST fits to concentration versus time data of all organic compounds comprising each reaction set. Uncertainties indicate 95% confidence intervals.

Reactants (HMO Age, Days)	Medium	Normalized Rate Constants ($M^{-1}hr^{-1}$)
50 μM Mandelic Acid 100 μM HMO-A(2)	5 mM Acetate (pH 4.0) 10 mM NaCl	$k_1' = 2.52\ (\pm 0.99) \times 10^2$ $k_2' = 8.61\ (\pm 1.77) \times 10^1$ $k_3' = 1.14\ (\pm 0.61) \times 10^2$ $k_4' = \sim 0$ $(k_1' + k_2') = 3.38\ (\pm 1.19) \times 10^2$ $[4.98\ (\pm 0.28) \times 10^2]$
50 μM Mandelic Acid 200 μM HMO-A(8)	5 mM Acetate (pH 4.0) 10 mM NaCl	$k_1' = 3.13\ (\pm 0.78) \times 10^2$ $k_2' = 1.20\ (\pm 0.32) \times 10^2$ $k_3' = 1.22\ (\pm 0.54) \times 10^2$ $k_4' = 3.02\ (\pm 0.66) \times 10^0$ $(k_1' + k_2') = 4.33\ (\pm 1.83) \times 10^2$ $[5.30\ (\pm 0.50) \times 10^2]$
50 μM Mandelic Acid 500 μM HMO-B(2)	5 mM Acetate (pH 4.0) 10 mM NaCl	$k_1' = 3.80\ (\pm 0.24) \times 10^2$ $k_2' = 1.58\ (\pm 0.19) \times 10^2$ $k_3' = 1.40\ (\pm 0.08) \times 10^2$ $k_4' = 4.12\ (\pm 0.44) \times 10^0$ $(k_1' + k_2') = 5.38\ (\pm 0.43) \times 10^2$ $[5.12\ (\pm 0.14) \times 10^2]$
50 μM Mandelic Acid 500 μM HMO-F(2)	5 mM Acetate (pH 4.0) 10 mM NaCl	$k_1' = 3.78\ (\pm 0.25) \times 10^2$ $k_2' = 1.62\ (\pm 0.21) \times 10^2$ $k_3' = 1.36\ (\pm 0.11) \times 10^2$ $k_4' = 4.13\ (\pm 0.39) \times 10^0$ $(k_1' + k_2') = 5.40\ (\pm 0.46) \times 10^2$ $[5.12\ (\pm 0.16) \times 10^2]$

50 μM Mandelic Acid 500 μM HMO-F(2)	5 mM Acetate (pH 4.0) 500 μM PO_4^{3-} 10 mM NaCl	$k_1' = 1.96\ (\pm 0.56) \times 10^2$ $k_2' = 8.03\ (\pm 1.09) \times 10^1$ $k_3' = 6.22\ (\pm 2.13) \times 10^1$ $k_4' = 4.12\ (\pm 1.88) \times 10^0$ $(k_1' + k_2') = 2.76\ (\pm 0.67) \times 10^2$ $[2.72\ (\pm 0.59) \times 10^2]$
50 μM Mandelic Acid 500 μM HMO-F(2)	5 mM Acetate (pH 4.0) 500 μM $P_2O_7^{4-}$ 10 mM NaCl	$k_1' = 7.80\ (\pm 2.20) \times 10^1$ $k_2' = 2.81\ (\pm 0.58) \times 10^1$ $k_3' = 2.41\ (\pm 1.44) \times 10^1$ $k_4' = \sim 0$ $(k_1' + k_2') = 1.06\ (\pm 0.29) \times 10^2$ $[1.07\ (\pm 0.01) \times 10^2]$
50 μM Mandelic Acid 500 μM HMO-D(2)	2 mM MOPS (pH 7.0) 15 mM I (using NaCl)	$(k_1' + k_2') = [9.78\ (\pm 0.21) \times 10^0]$
50 μM Mandelic Acid 500 μM HMO-D(2)	2 mM PO_4^{3-} (pH 7.0) 15 mM I (using NaCl)	$(k_1' + k_2') = [1.08\ (\pm 0.03) \times 10^1]$
50 μM Mandelic Acid 500 μM HMO-D(2)	2 mM $P_2O_7^{4-}$ (pH 7.0) 15 mM I (using NaCl)	$(k_1' + k_2') = [1.54\ (\pm 0.07) \times 10^1]$
50 μM Phenylglyoxylic Acid 500 μM HMO-C(10)	5 mM Acetate (pH 4.0) 10 mM NaCl	$k_3' = 1.49\ (\pm 0.17) \times 10^2$ $[1.47\ (\pm 0.06) \times 10^2]$
50 μM Benzaldehyde 500 μM HMO-G(3)	5 mM Acetate (pH 4.0) 10 mM NaCl	$k_4' = 4.50\ (\pm 0.58) \times 10^0$ $[4.43\ (\pm 0.41) \times 10^0]$
50 μM Phenyllactic Acid 500 μM HMO-C(3)	5 mM Acetate (pH 4.0) 10 mM NaCl	$(k_1' + k_2') = [7.22\ (\pm 0.32) \times 10^1]$
50 μM Phenylpyruvic Acid 500 μM HMO-H(5)	5 mM Acetate (pH 4.0) 10 mM NaCl	$k_3' = [1.86\ (\pm 0.79) \times 10^3]$
50 μM Phenylacetaldehyde 500 μM HMO-G(3)	5 mM Acetate (pH 4.0) 10 mM NaCl	$k_4' > [4.69 \times 10^5]$
50 μM Phenyllactic Acid	2 mM MOPS (pH 7.0)	$k_1' + k_2' = [1.86\ (\pm 0.34) \times 10^0]$

500 μM HMO-E(3)	15 mM I (using NaCl)	
50 μM Phenyllactic Acid 500 μM HMO-E(3)	2 mM PO_4^{3-} (pH 7.0) 15 mM I (using NaCl)	$k_1' + k_2' = [2.66\ (\pm 0.29) \times 10^0]$
50 μM Phenyllactic Acid 500 μM HMO-E(3)	2 mM $P_2O_7^{4-}$ (pH 7.0) 15 mM I (using NaCl)	$k_1' + k_2' = [3.78\ (\pm 0.14) \times 10^0]$

661

Hydroxy Acid Reaction Set

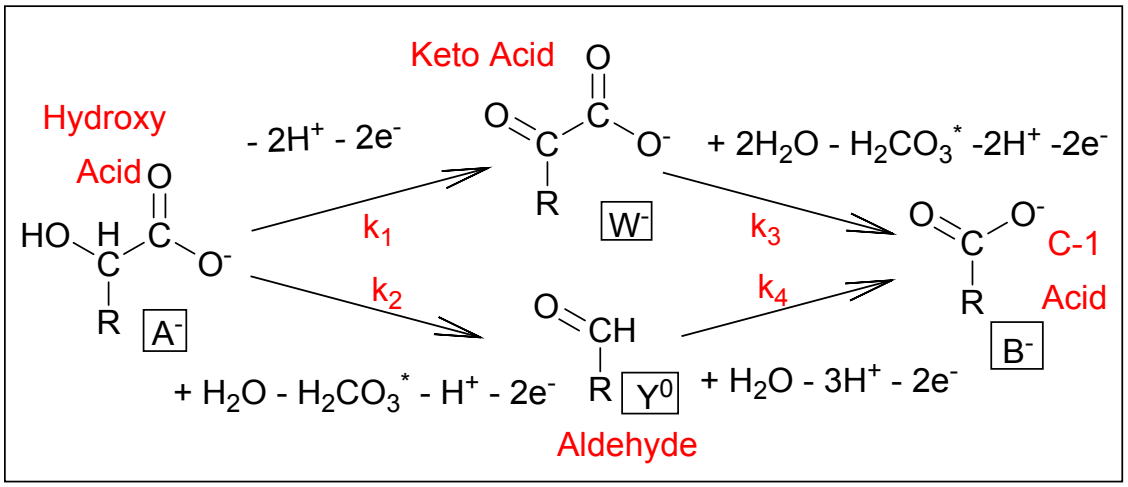

R = 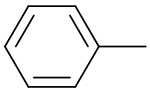	HA^0	HW^0	HB^0
	Mandelic Acid	Phenylglyoxylic Acid	Benzoic Acid
		Y^0	
		Benzaldehyde	
R = 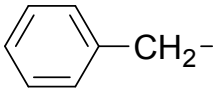	HA^0	HW^0	HB^0
	Phenyllactic Acid	Phenylpyruvic Acid	Phenylacetic Acid
		Y^0	
		Phenylacetaldehyde	

Figure 1. Pathways for hydroxy acid oxidation. Hydration and enolization reactions for the keto acid and aldehyde intermediates are also shown.

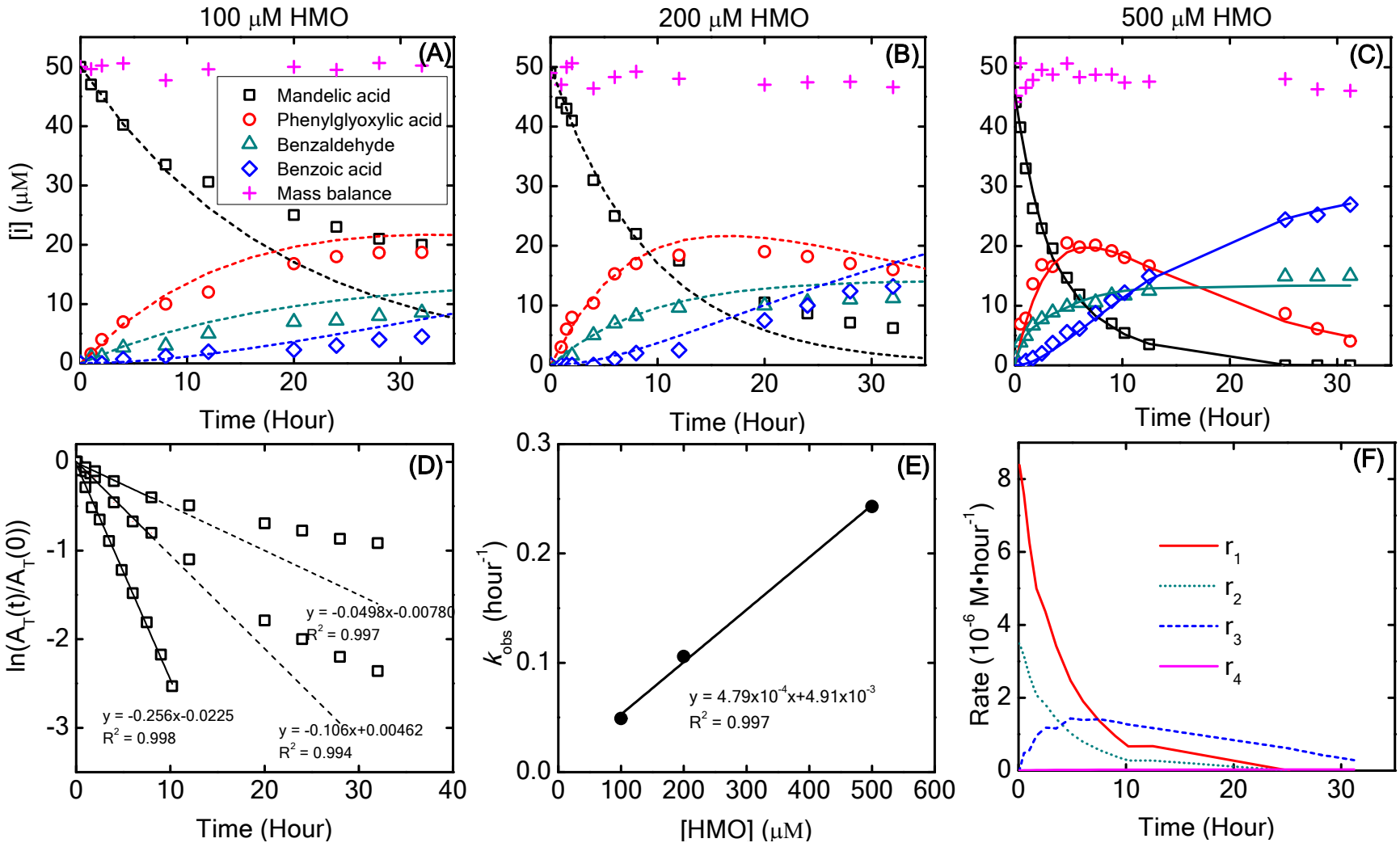

Figure 2. Oxidation of 50 μM mandelic acid by (A) 100 μM, (B) 200 μM, and (C) 500 μM HMO. Phenylglyoxylic acid, benzaldehyde, and benzoic acid products are also shown. (D) Semi-log plots for mandelic acid loss for the three HMO loadings. Fitting was applied to the data delineated by continuous lines; dashed lines are extrapolated. (E) First-order rate constants for mandelic

acid loss as a function of HMO loading. (F) Rates of contributing reactions calculated for 500 μM HMO, based on the numerical approach described in the text. Reaction medium: 5.0 mM acetate buffer (pH 4.0), and 10 mM NaCl.

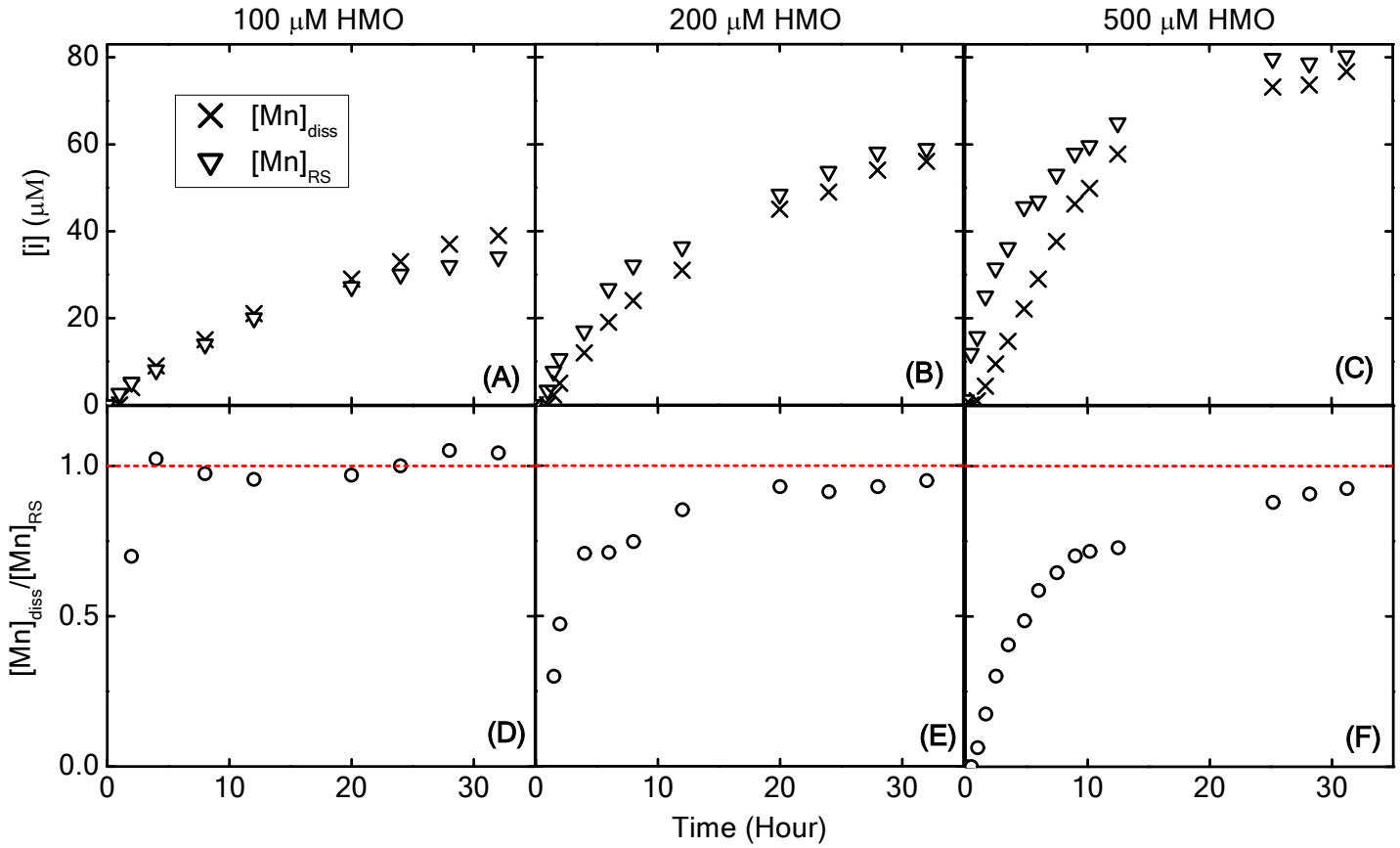

Figure 3. Using reaction stoichiometry to evaluate the oxidation of 50 μM mandelic acid by (A, D) 100 μM, (B, E) 200 μM, and (C, F) 500 μM HMO. Upper plots: $[Mn]_{diss}$ (×) refers to dissolved Mn measured by filtration and AAS. $[Mn]_{RS}$ (▽) is calculated from measurements of A_T, W_T, Y_T, and B_T (reaction set organic compounds), and expected reaction stoichiometries as discussed in the text. Lower plots: $[Mn]_{diss}/[Mn]_{RS}$ as a function of time. Reaction conditions: 5 mM acetate buffer (pH 4.0), and 10 mM NaCl.

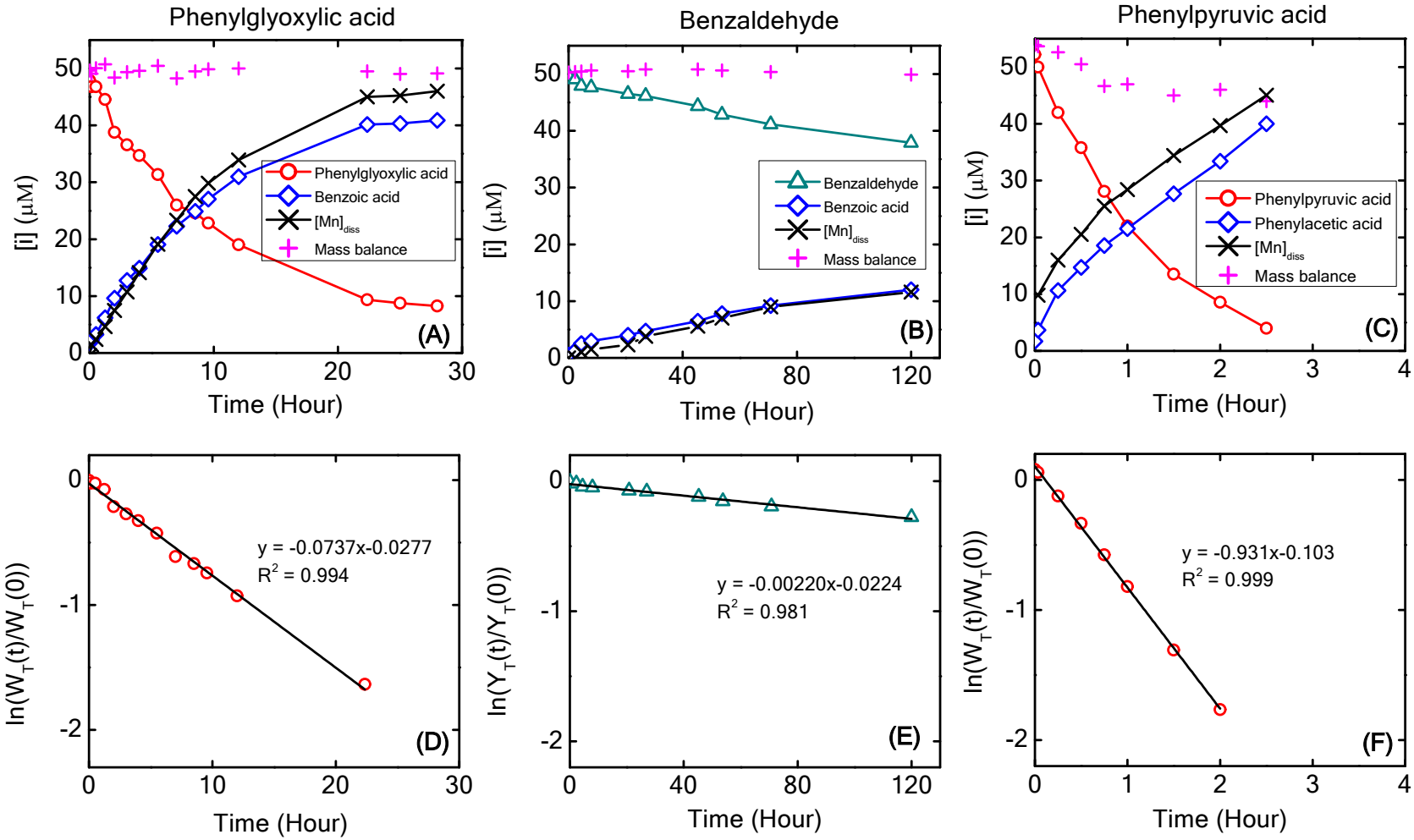

Figure 4. Using keto acids and aldehydes as substrates. Phenylglyoxylic acid (A) and benzaldehyde (B) are from the mandelic acid reaction set, while phenylpyruvic acid (C) is from the phenyllactic acid reaction set. Corresponding semi-log plots for loss of substrate are shown in D-F. Reaction conditions: 50 μM substrate, 500 μM HMO, 5 mM acetate buffer (pH 4.0), and 10 mM NaCl.

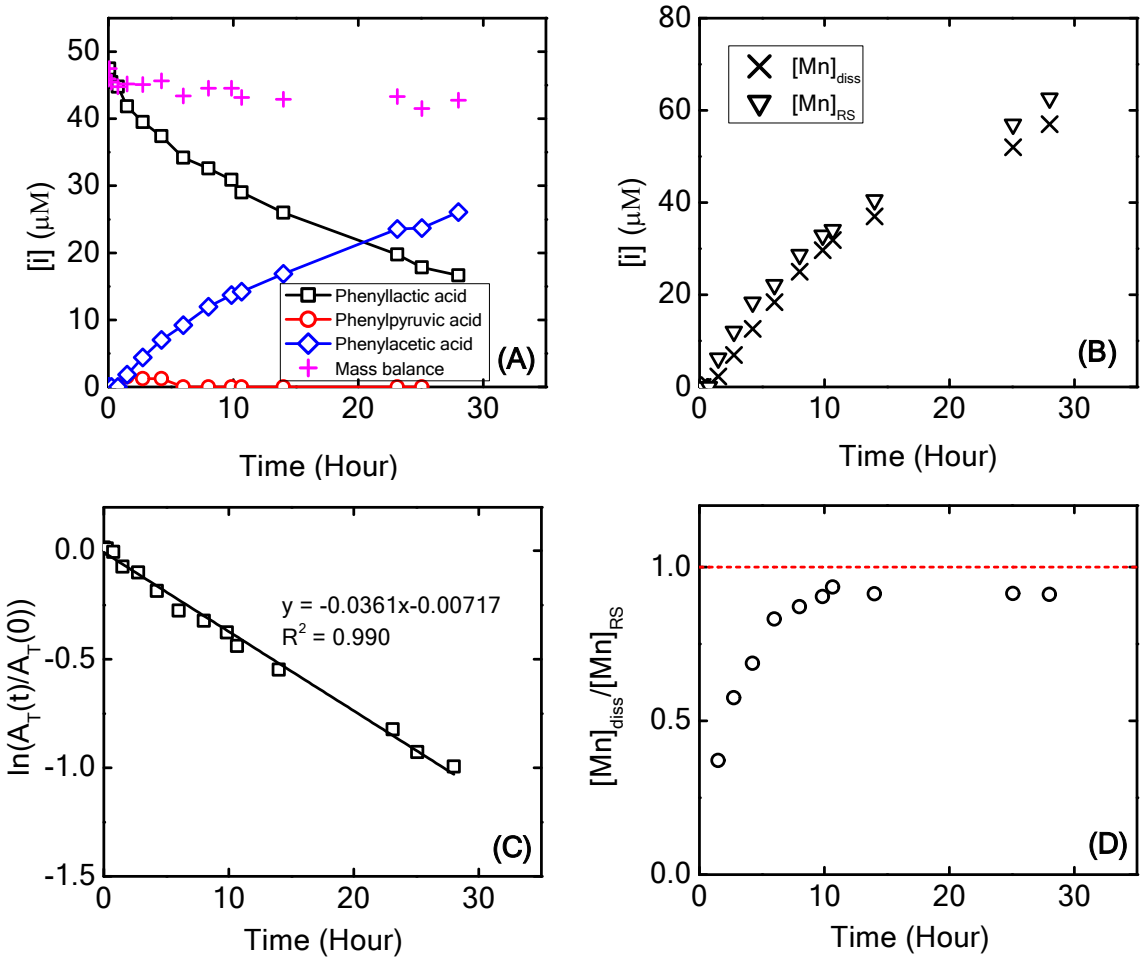

Figure 5. Oxidation of 50 μM phenyllactic acid by 500 μM HMO at pH 4.0 (5.0 mM acetate buffer, 10 mM NaCl). (A) and (B) are time course results, while (C) is a semi-log plot for phenyllactic acid loss. (D) explores reaction stoichiometry using $[Mn]_{diss}/[Mn]_{RS}$ ratios.

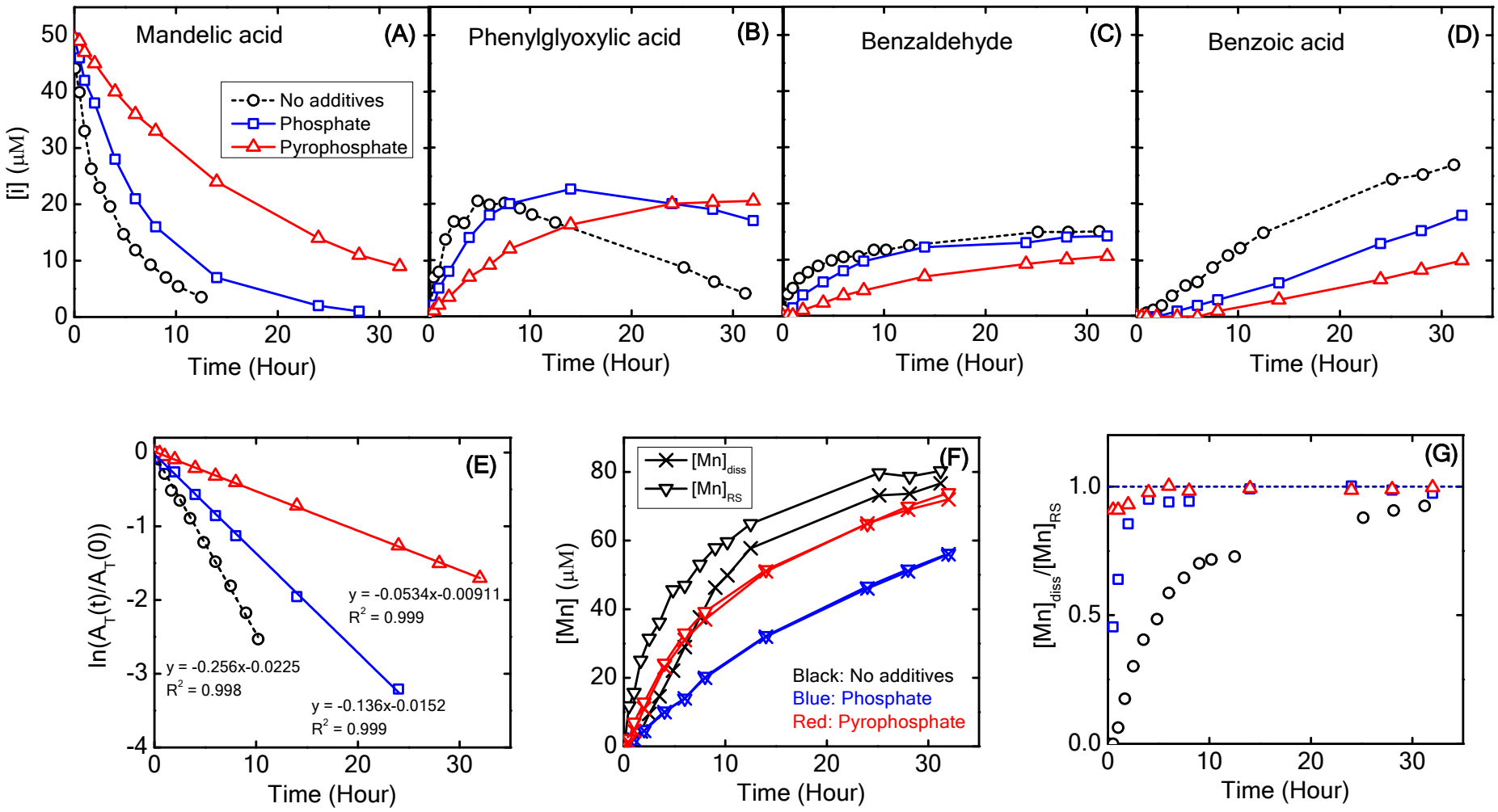

Figure 6. pH 4.0 experiments examining the effects of adding 500 μM phosphate or pyrophosphate on the reaction of mandelic acid with HMO. (A) Mandelic acid, (B) phenylglyoxylic acid, (C) benzaldehyde, and (D) benzoic acid product time course plots. (E) Semi-log plots for mandelic acid loss. (F) $[Mn]_{diss}$ and $[Mn]_{RS}$ and (G) $[Mn]_{diss}/[Mn]_{RS}$ as a function of time.

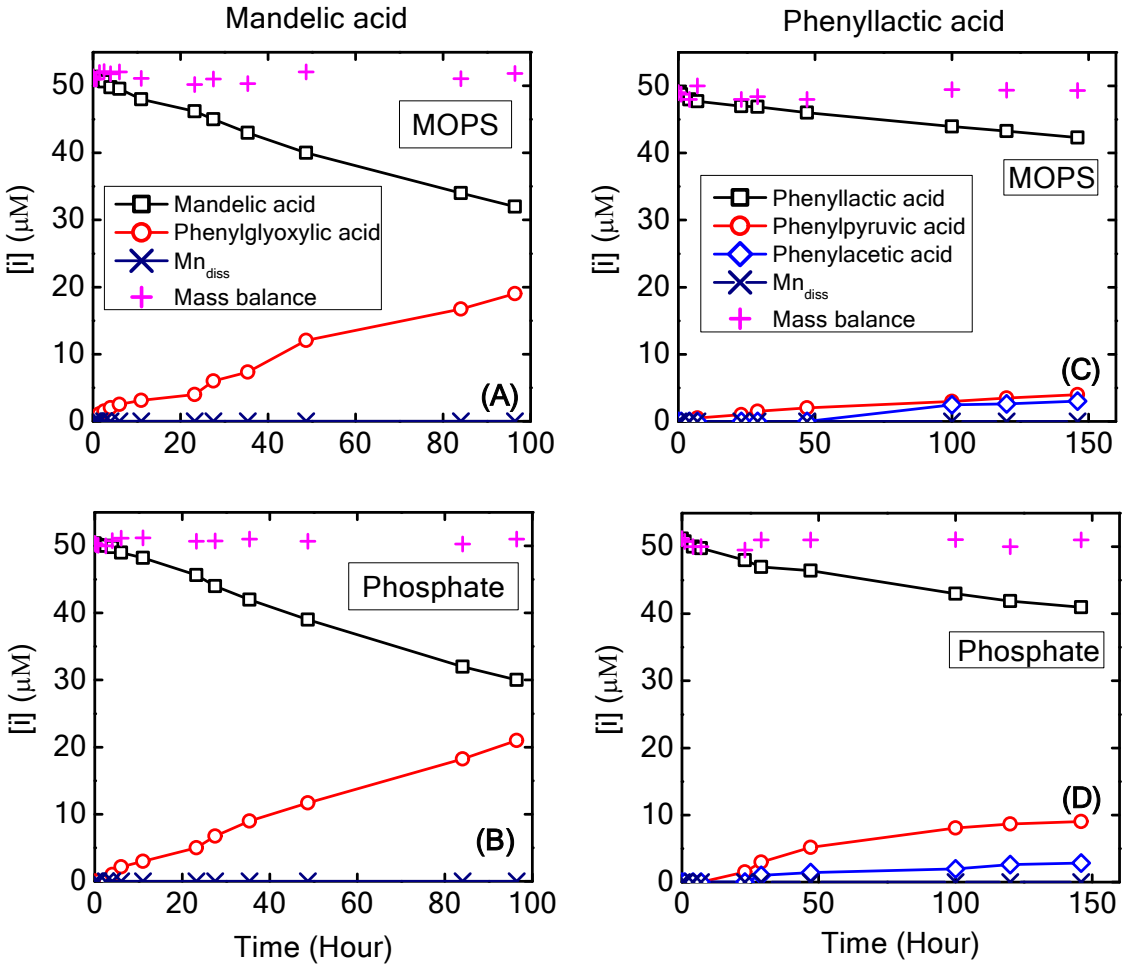

Figure 7. pH 7.0 experiments. Oxidation of 50 μM (A-B) mandelic acid or (C-D) phenyllactic acid by 500 μM HMO medium employing 2.0 mM MOPS or phosphate buffer. An ionic strength of 15 mM was fixed using NaCl addition.

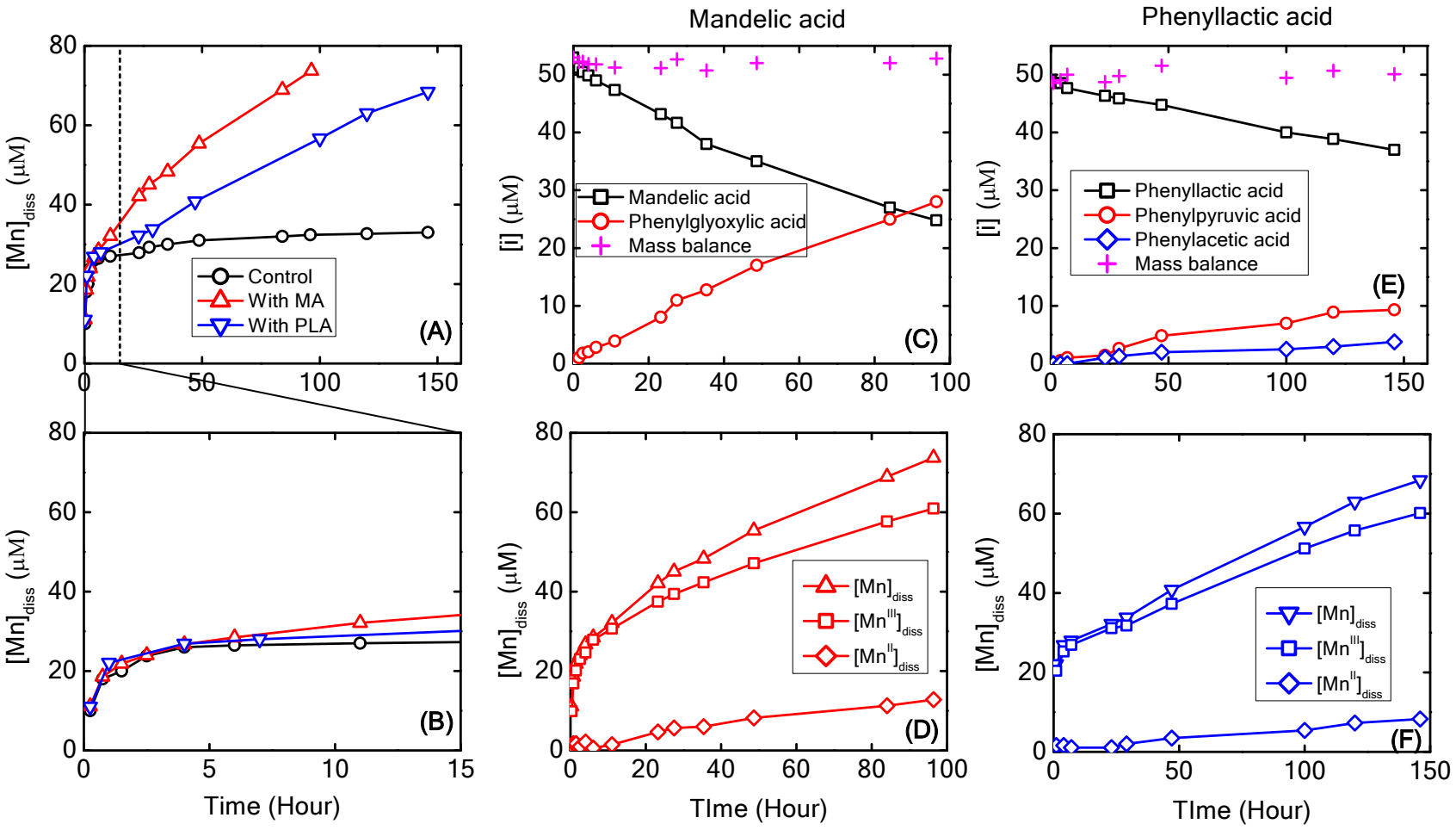

Figure 8. pH 7.0 experiments employing 2 mM pyrophosphate buffer. Reactions were performed in substrate-free suspension (control) or in suspensions containing 50 μM mandelic acid (MA) or phenyllactic acid (PLA). Suspensions all contained 500 μM HMO. An ionic strength of 15 mM was fixed using NaCl addition. (A-B) Concentrations of dissolved Mn in 150 hours and the first 15 hours. (C) and (E) show concentrations of organic substrates. (D) and (F) show concentrations of dissolved Mn^{II} and Mn^{III}.